Proceedings of the 6th International Conference on the Application of Physical Modelling in Coastal and Port Engineering and Science (Coastlab16)

Ottawa, Canada, May 10-13, 2016

LABORATORY AND FIELD INVESTIGATIONS OF WAVE ATTENUATION BY LIVE MARSH VEGETATION

WEIMING WU[1], YAVUZ OZEREN[2], QIN CHEN[3], RANJIT JADHAV[4], DANIEL WREN[5]

1 Department of Civil and Environmental Engineering, Clarkson University, NY, USA, wwu@clarkson.edu

2 National Center for Computational Hydroscience and Eng., The University of Mississippi, USA, yozeren@ncche.olemiss.edu

3 Department of Civil and Environ. Engineering, Louisiana State University, LA, USA, qchen@lsu.edu

4 FTN Associates, Ltd., 10508 North Glenstone Place, Baton Rouge, LA, USA, rsj@ftn-assoc.com

5 National Sedimentation Laboratory, USDA-ARS, daniel.wren@ars.usda.gov

ABSTRACT

Wave attenuation by live marsh vegetation was investigated experimentally in this study. Laboratory experiments were conducted in a 20.6 m long, 0.69 m wide and 1.22 m deep wave flume under regular and random waves. The vegetation species used are *Spartina alterniflora* and *Juncus roemerianus*, which widely exist along the U.S. coastlines. Field measurements were conducted under high-energy conditions during a tropical storm at a salt marsh in Terrebonne Bay on the Louisiana coast of the Gulf of Mexico. The field site was dominated by *S. alterniflora*. The wave attenuation data were compared against an analytical model, and the bulk drag coefficient of vegetation was then calibrated in each experiment run. The drag coefficient of *S. alterniflora* is found to be a function of the Keulegan-Carpenter number, whereas the drag coefficient of *J. roemerianus* is closely related to the Keulegan-Carpenter number and vegetation submergence (ratio of vegetation height and water depth). The importance of submergence for *J. roemerianus* is due to that its stem diameter and density vary along elevation. It is recognized that the data using regular and random waves collapse into single relation for each species by using significant wave height and peak wave period as the representative parameters in the Keulegan-Carpenter number.

KEYWORDS: Marsh vegetation, wave attenuation, regular waves, random waves, drag coefficient.

1 INTRODUCTION

Surge and waves generated by hurricanes and other severe storms can cause devastating damage of property and loss of life in coastal areas. Vegetation in wetlands, coastal fringes and stream floodplains can reduce storm surge and waves while providing ecological benefits and complementing traditional coastal defense approaches such as permanent levees, seawalls and gates. However, how to quantify surge and wave reduction needs more investigations.

Several theoretical studies were carried out on wave attenuation by vegetation. Dalrymple et al. (1984) presented the first theoretical model of wave energy dissipation assuming plants as rigid cylinders that exert drag force on monochromatic waves. The Dalrymple et al. (1984) formulation was extended by Mendez et al. (1999) and Mendez and Losada (2004) for irregular waves. Kobayashi et al. (1993) presented an approach based on continuity and momentum equations demonstrating exponential wave height decay. Chen and Zhao (2012) proposed models on random wave energy dissipation based on the joint probability distribution of wave heights and wave periods. Lowe et al. (2005, 2007) developed a theoretical model of monochromatic wave flow structure inside a model canopy of rigid cylinders based on momentum balance and extended the model to random wave conditions. Mullarney and Henderson (2010) investigated the wave-vegetation interaction and derived an analytical model for the wave-induced movement of single-stem vegetation treated as an Euler-Bernoulli problem for a cantilevered beam.

Wave propagation through water body with vegetation has been studied in controlled laboratory environments by Dubi and Tørum (1996), Løvås and Tørum (2001), Augustin et al. (2009), Chakrabarti et al. (2011), and Stratigaki et al. (2011), among others. Field investigations of waves over vegetation have been carried out for salt marshes (Möller et al., 1999; Möller and Spencer, 2002; Cooper, 2005; Möller, 2006; Bradley and Houser, 2009; Mullarney and Henderson, 2010), coastal

mangrove forests (Mazda et al., 2006; Quartel et al., 2007), and vegetated lakeshores (Lövstedt and Larson, 2010). All these studies show that wave energy can be attenuated by vegetation, and the effectiveness of attenuation depends on vegetation types and wave environment.

To understand and quantify the attenuation of waves by live marsh vegetation, a series of laboratory experiments and field observations were conducted in this study. Two marsh vegetation species commonly distributing along the U.S. coastlines were selected. A large number of data were collected to develop formulas for the drag coefficient of the tested species.

2 LABORATORY EXPERIMENTS

Experiments were conducted in a 20.6 m long, 0.69 m wide and 1.22 m deep wave flume (Figure 1). The bottom of the wave flume was elevated 0.29 m by a plywood false floor to facilitate the placement of vegetation. A ramp with a slope of 1/7 was built in front of the wave generator to provide a gradual transition up to the false floor. A porous, parabolic wave absorber was constructed at the downwave end of the flume to minimize wave reflection. The effective length of the flume from the wave generator to the toe of the absorber was 16.9 m. A 3.6 m long test section was placed 11.5 m away from the wave generator. Tape water was used in the experiments, and the water temperature varied between 20–24ºC.

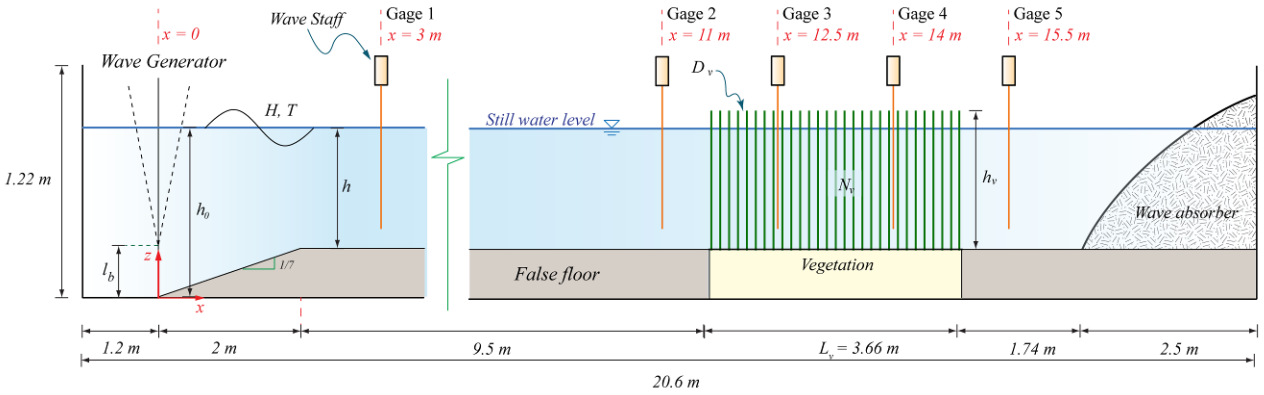

Figure 1. Definition sketch of the experimental setup.

The studied marsh vegetation species were *Spartina alterniflora* Loisel. (smooth cordgrass) and *Juncus roemerianus* Scheele. (black needlegrass rush) (Figure 2). Both are perennial emergent grasses and widely distribute along the U.S. coastlines. Pennings et al. (2005) investigated the factors producing zonation patterns of the dominant plants in salt marshes in south-eastern U.S., and found that *J. roemerianus* dominates the high marsh and *S. alterniflora* dominates the middle and low marsh. We collected samples of *S. alterniflora* from Terrebonne Bay, Louisiana and Grand Bay, Mississippi, USA and *J. roemerianus* from Grand Bay, Mississippi, USA, and measured the geometric properties of these plants to provide initial data for the design of the experiments.

Green *S. alterniflora* and *J. roemerianus* used in the experiments were obtained from an outdoor nursery near Houma, Louisiana, USA. They were transferred to the laboratory in six custom-built PVC boxes. The boxes were 68 cm wide, 61 cm long and 21 cm deep. Each box contained sixteen rectangular cells that measured 17 cm by 15 cm. Plugs of vegetation with an approximately equal number of stems were placed into each cell to provide an even distribution and control the stem density. The remaining gap around the plugs was filled with native soil. After being installed in the wave flume, the plants were irradiated by three 750 W growing lights for 10 hours per day for a 30 day period. The wave flume was filled with fresh water to just above the soil level during this recovery period. For each live vegetation species tested in the flume, vegetation density (N_v), stem height (h_v) and diameter (D_v) were measured (Table 1). The vegetation densities in Table 1 are typical values observed on the aforementioned sites of the Louisiana and Mississippi coasts (Wu et al., 2011, 2012).

Five capacitance-type wave probes were used to measure water surface displacement. The sampling rate of the wave probes was 30 Hz, and the spatial resolution was 0.24 mm. The probes were calibrated in the wave flume with a point gauge to ensure accurate water level measurements, and the calibrations were checked several times during the study. One of the probes was placed 3 m from the paddle to measure the incident wave height, and the remaining four were distributed along the test section at 1.5 m intervals starting 0.5 m upwave of the vegetation field (Figure 1).

Wave generation and data collection were controlled by a computer, which enabled automation of multiple experiments. Regular and random waves were used in the experiments. For each vegetation configuration, a range of combinations of wave height, period, and water depth was used. The still water level was measured with a point gauge before each set of experiments and used later for calibration. Regular wave experiments were run for at least 100 wave cycles and each experiment was

repeated three times. Reference runs without vegetation were also performed for the same wave properties as used with vegetation. Irregular waves were generated using a set of JONSWAP spectra. Five $100T_p$ long irregular time series signals were established for each spectrum to generate approximately 500 waves for each condition, where T_p is the peak wave period. The five sets of wave spectra corresponding to the recorded wave height time series at each gauge were averaged in the frequency domain, and the average wave spectrum was used to calculate wave properties.

(a)  (b) 

Figure 2. Studied vegetation species: (a) *Spartina alterniflora* Loisel. (Wikipedia, 2016), and (b) *Juncus roemerianus* Scheele. (University of Florida, 2016)

Table 1. Properties of vegetation used in the lab experiments.

Vegetation type	Density N_v (m^{-2})	Stem height h_v (m)	Stem diameter D_v (mm)
S. alterniflora	405	0.59± 0.21	6.5±0.9
J. roemerianus	2857	1.03±0.27	2.4±0.6

The zero down-crossing method was used to evaluate the wave heights and wave periods for regular waves. The individual wave heights were defined as the difference between the highest and lowest water surface readings between two zero down-crossing points. For irregular waves, periods were obtained through spectral analysis by using a Fast Fourier Transform (FFT) routine. The peak wave period, T_p, which is the reciprocal of the spectral frequency at the maximum spectral density, was used as the wave period. The energy based significant wave height is defined by the square root of zero-th moment of the energy spectrum (Longuet-Higgins 1952) as follows:

$$H_{mo} = 4.0\sqrt{m_0} \tag{1}$$

where m_0 is the zero-th moment of the wave spectrum. The wave properties used in the laboratory experiments are shown in Table 2.

Table 2. Wave conditions in the lab experiments.

	Regular waves	Irregular waves
Wave height - H_i (H_{mo}) (m)	0.02 – 0.15	0.02 – 0.10
Wave period - T (T_p) (s)	0.7 – 2.0	0.7 – 1.8
Water depth - h (m)	0.4 – 0.7	0.5 – 0.7

3 FIELD MEASUREMENTS

Wave data were collected over a two-day period (September 3-4, 2011) at a salt marsh wetland in Terrebonne Bay on the Louisiana coast of the Gulf of Mexico during Tropical Storm Lee. Situated in the Mississippi River delta, Terrebonne Bay is a shallow estuary bounded by the natural levees of Bayou Terrebonne on the east, and the Houma Navigation Canal on the west. Salt marshes line the upper portion of the bay, where vegetation communities include smooth cordgrass (*Spartina*

alterniflora) and salt marsh meadow (*Spartina patens*). On the south, the bay is bordered by a series of narrow, low-lying barrier islands. The wave environment in the bay is generally comprised of locally generated seas, but offshore swell waves also propagate inwards through the gaps in the barrier island chain, or when the barrier islands are flooded by a tropical storm surge. The region has a micro-tidal environment (tidal range < 0.5 m) and depths in the bay vary from 1 to 3 m. The southern fetch varies from 10 to 24 km. The region experiences annual winter cold weather fronts, and surge and waves from tropical cyclones.

The marsh site selected for the field study is a vegetated platform wetland with a shallow bay on the windward (south) side (Figure 3). On the leeward (north) side the marsh extends for a distance of about 500 m, beyond which lies open water of the bay. A field topographic survey along a north-south transect shows a very low berm near the southern edge from where the marsh floor gently slopes inland. The southern marsh edge, where the incident waves first landed, has an approximate east-west alignment. The shore-normal direction has a bearing of 20°. Five wave gages (pressure transducers W0 through W4) were deployed along a north-south transect nearly perpendicular to the marsh edge. Gage W0 was located in the open water on the up-wave (south) side of the marsh about 45 m away at a depth of about 1.4 m below the mean sea level, to measure incoming wave energy. Gage W1 was the first gage on the marsh that encountered incident waves. This gage was placed more than 16 m inwards (north) of the marsh edge to avoid the breaking zone created by waves breaking at the marsh edge. The post-cyclone survey of the site showed vegetation and surface damage within 8 to 10 m of the edge. The remaining three gages, W2, W3 and W4, were further inland; gage W4 being the farthest north at 43.8 m from the first marsh gage W1. All gages were self-logging pressure sensors that sampled continuously at 10 Hz over the duration of the storm. The sensors were encased in a heavy metal base to ensure stability under passing waves.

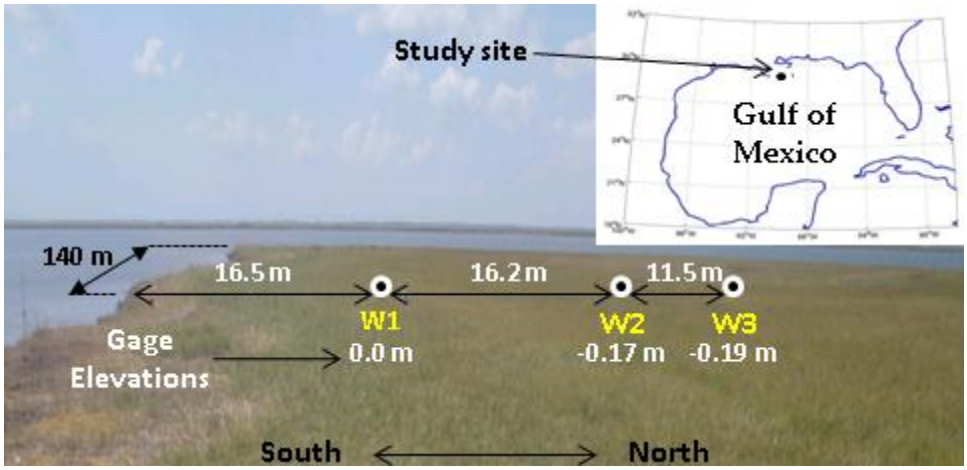

Figure 3. Study area location (Terrebonne Bay, Louisiana) and the schematic of experimental set up showing wave gages (W1-W3). Gage elevations relative to gage W1. Not to scale.

The dominant vegetation at the site is *Spartina alterniflora*. This plant typically has a thick stem, with tapering flexible narrow blades. Vegetation properties were measured 11 days after the storm. Stem population density N_v, stem height h_v, total plant height h_{vt}, stem diameter D_v, and Young's Modulus E_v were measured at one location each between gages W1-W2 and W2-W3. The population density is the number of stems in one meter square area. The stem height is defined as the length between the plant base and the location of the topmost blade along the stem. The total plant height is defined as the length between the plant base and the tip of the plant with all blades aligned along the stem. The representative diameter of the plant was measured at one-fourth the stem height. The Young's Modulus was determined from measuring force required to bend the stem in the field from a certain height by a known angle and applying the Euler-Bernoulli beam theory. All above parameters were measured for 14 plants at each location. The mean and standard deviation of the measurements collected from the sites between gages W1 and W2 and between gages W2 and W3 are given in Table 3.

Table 3. Properties of vegetation in the field measurements (mean and standard deviation).

Site	Density N_v (m^{-2})	Stem height h_v (m)	Total plant height h_{vt} (m)	Stem diameter D_v (mm)	Young's modulus E_v (MPa)
Between W1 and W2	424	0.21±0.04	0.62±0.05	8.0±1.1	80±27
Between W2 and W3	420	0.23±0.06	0.63±0.11	7.5±1.3	79±32

The wave energy spectra and the integral wave parameters were calculated using standard spectral analysis. The measured continuous pressure time series was first divided into consecutive segments or bursts of 15 minutes. For each burst, the spectral

density of pressure, S_p, was calculated using Welch's periodogram method (e.g., Bendat and Piersol, 2000). The pressure spectra were transferred to wave energy spectra, S_e, using the linear wave theory. The spectral energy above 0.7 Hz is generally less than 5% of the total energy, so it was excluded. The significant wave height was calculated using Equation (1) and the root-mean-squared (RMS) wave height, $H_{rms} = 2\sqrt{2m_0}$. The observed wave parameters are given in Table 4.

All measurements recorded when the water depth was less than 0.4 m were eliminated, because the wave energy was found to be negligible at these levels. Thus, the study represents submerged vegetation conditions only. In the last gage segment, between W3 and W4, the characteristic exponential energy dissipation due to vegetation was observed during only 5 bursts. Therefore, the entire dataset from gage W4 was not used in this analysis. The wave energy losses due to vegetation were considered dominant compared to the other source terms. To ascertain the validity of this assumption, the relative magnitude of source terms of the local wave generation and the losses due to bottom-friction, white-capping, and depth-limited breaking were evaluated. The wave records with significant potential for these source terms were removed. Details of wave data analysis are reported in Wu et al. (2011, 2012).

Table 4. Range and mean (in parentheses) of wave parameters in the field measurements.

Parameter	Gage W1	Gage W2	Gage W3
Depth, h (m)	0.40-0.82 (0.55)	0.57-1.0 (0.72)	0.57-1.01 (0.72)
Significant wave height, H_{m0} (m)	0.15-0.40 (0.24)	0.07-0.28 (0.14)	0.04-0.21 (0.09)
Peak wave period, T_p (s)	2.5-4.7 (4.0)	1.2-4.5 (2.3)	1.3-4.5 (2.6)
Relative wave height, H_{m0}/h	0.36-0.49 (0.41)	0.12-0.29 (0.18)	0.08-0.22 (0.12)

4 ANALYTICAL MODEL OF WAVE ENERGY DISSIPATION BY VEGETATION

As waves travel through a waver body with vegetation, their energy changes due to local wave generation, white-capping, depth-limited breaking, bed friction and vegetation resistance. Among all these sources/sinks, the vegetation resistance is usually dominant. Therefore, the energy balance equation of monochromatic (regular) waves can be written as

$$\frac{\partial\left(C_g E\right)}{\partial x} = -S_v \tag{2}$$

where x is the cross-shore coordinate, E is the wave energy density, C_g is the group wave celerity, and S_v is the time averaged rate of energy dissipation due to vegetation per unit horizontal area. The energy loss due to vegetation can be approximated as (e.g., Dalrymple et al., 1984; Mendez and Loasada, 2004)

$$S_v = \frac{1}{T}\int_t^{t+T}\int_{-h}^{h_v-h} F_x u dz dt \tag{3}$$

where u is the wave velocity acting on the vegetation, and F_x is the drag force by the vegetation elements:

$$F_x = \frac{1}{2} C_D \rho D_v N_v u|u| \tag{4}$$

where C_D is the drag coefficient, and ρ is the water density. The drag coefficient for a single cylinder is related to the Reynolds number. For an array of vegetation elements, the bulk drag coefficient C_D is also related to other factors, such as geometrical and mechanic properties of vegetation.

For rigid vegetation over a flat bed, assuming linear wave theory and constant quantities over the depth, the regular wave height evolution can be written as (Dalrymple et al., 1984)

$$\frac{H}{H_i} = \frac{1}{1+\alpha x} \tag{5}$$

where H_i and H are the incident wave height and wave height in the vegetation zone, and α is a damping factor defined by

$$\alpha = \frac{4}{9\pi} H_i C_D D_v N_v k \frac{\sinh^3 kah + 3\sinh kah}{(\sinh 2kh + 2kh)\sinh kh} \tag{6}$$

where $a = h_v / h$ for submerged vegetation and unity for emergent vegetation. A similar relation can be established for irregular waves (Mendez and Loasada, 2004), which can be written as Equation (5) with H being replaced by the RMS wave height H_{rms} and the damping factor

$$\alpha = \frac{1}{3\sqrt{\pi}} H_{rmsi} C_D D_v N_v k_p \frac{\sinh^3 k_p ah + 3\sinh k_p ah}{(\sinh 2k_p h + 2k_p h)\sinh k_p h} \tag{7}$$

where k_p is the wave number associated with the peak period $k_p = 2\pi / L_p$.

5 DATA ANALYSES AND RESULTS

By using the profiles of wave height measured in each run of the lab experiments and field measurements, we can determine the decay rate coefficient α in Equation (6) or (7), and in turn the drag coefficient C_D. C_D is then related to the Reynolds number and Keulegan-Carpenter number. In this study, the Keulegan-Carpenter number is found to have good correlation with drag coefficient. It is defined as

$$K_c = \frac{u_c T}{D_v} \tag{8}$$

where T is the wave period,, and u_c is the characteristic velocity defined as the maximum horizontal velocity just before the vegetation zone at the height of the submerged portion of vegetation:

$$u_c = \frac{\pi H}{T} \frac{\cosh(kah)}{\sinh(kh)} \tag{9}$$

For the cases of regular waves, the wave height H and wave period T are used in Equation (9). For the cases of irregular waves, H may be replaced by the significant wave height H_{mo} or the RMS wave height H_{rms}, and T may be the peak wave period T_p or the mean wave period T_z. In this study, the significant wave height H_{mo} and the peak wave period T_p are used for H and T in Equation (9). Through this arrangement, the data of random and regular waves can collapse into single relation of C_D and K_C, as explained below for the two vegetation species *S. alterniflora* and *J. reomarianus*.

5.1 Spartina Alterniflora

Figure 4 shows the relation of C_D and K_C derived from all the laboratory and field data for live (green) *S. alterniflora*. The waves encountered in the field measurement are random waves, whereas the waves used in the laboratory experiments are both regular and random. One can see that the data from regular and random waves closely distribute along a single strip. Because the waves in the field measurements have higher wave heights and longer wave periods, the field data have larger K_C than the laboratory experiment data. The general trend of all the laboratory and field data ($3.6<K_C<250$) can be represented by the following regression equation:

$$C_D = 0.825 + \frac{665}{K_C^{1.4}} \tag{10}$$

The coefficient of correlation, R^2, is 0.906 for Equation (10). The other performance statistics used include the root-mean-square error and bias defined as

$$\log(E_{rms}) = \sqrt{\frac{1}{N}\sum_{i=1}^{N}\left[\log\left(\frac{C_{D,\text{predicted}}}{C_{D,\text{measured}}}\right)\right]^2} \tag{11}$$

$$\log(bias) = \frac{1}{N}\sum_{i=1}^{N}\log\left(\frac{C_{D,\text{predicted}}}{C_{D,\text{measured}}}\right) \tag{12}$$

The log(*bias*) and log(E_{rms}) are -0.00009 and 0.108, respectively, for Equation (10). These statistics indicate that the drag coefficient is highly related to the Keulegan-Carpenter number, and Equation (10) represents well the relationship of C_D and K_C for live *S. alterniflora*.

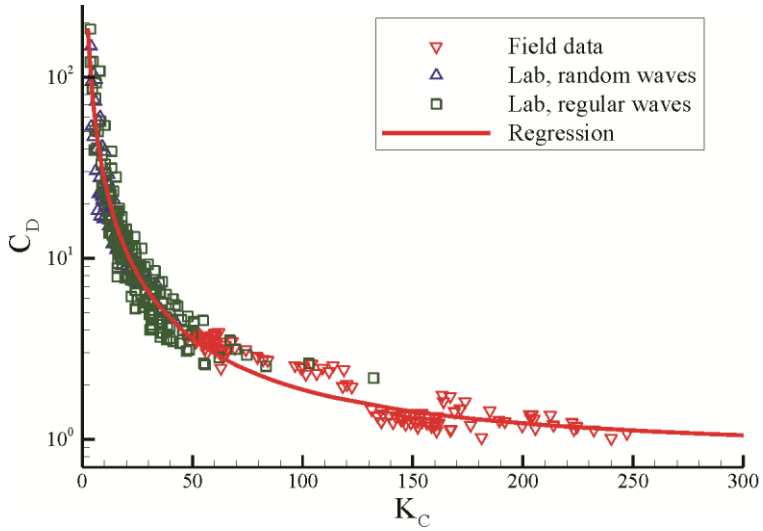

Figure 4. Relationship of drag coefficient and Keulegan-Carpenter number for *S. alterniflora*.

5.2 Juncus Roemerianus

Figure 5 shows the relation of C_D and K_C for live (green) *J. roemerianus* based on the data collected in the lab experiments. No field data are obtained for this vegetation species. Unlike the case of *S. alterniflora*, the measured data of *J. roemerianus* scatter widely and do not support a single relation between C_D and K_C. After carefully checking the data, it is found that the drag coefficient of *J. roemerianus* is also related to the relative vegetation height h_v/h. The reason is that stem diameter and density of *J. roemerianus* vary along elevation (Ozeren et al., 2015). Therefore, the data are reanalyzed by changing the independent variable as $K_C(h_v/h)^{-2}$. Figure 6 shows the relation of C_D and $K_C(h_v/h)^{-2}$, including the data of regular and random waves. All the data collapse to a single relation which is represented by the following regression equation:

$$C_D = \frac{33.7}{\left[K_C\left(h_v/h\right)^{-2}\right]^{0.915}} \tag{13}$$

Equation (13) has a R^2 of 0.903, log(*bias*) of -0.0017, and log(E_{rms}) of 0.080. The data in Figure 6 covers $1.47<h_v/h<2.58$ and $4.5<K_C<280$.

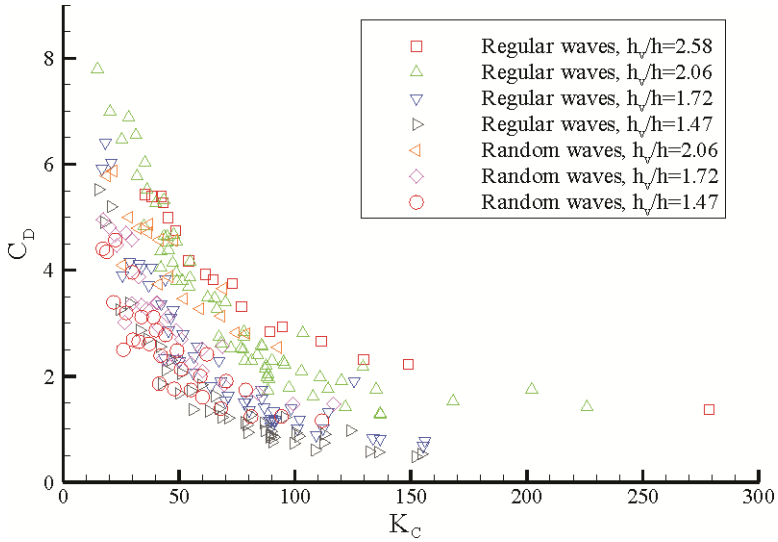

Figure 5. Relationship of drag coefficient and Keulegan-Carpenter number for *J. roemerianus*.

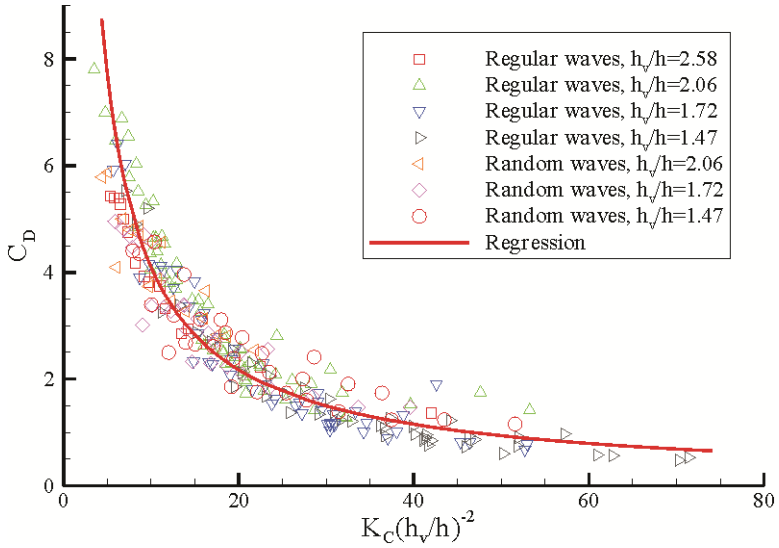

Figure 6. Drag coefficient as function of Keulegan-Carpenter number and relative vegetation height for *J. roemerianus*.

5.3 Comparison of Drag Coefficients of S. alterniflora and *J. roemerianus*

The drag coefficients of *S. alterniflora* and *J. roemerianus* are compared in Figure 7. For more clear view, only the C_D-K_C regression relation of *S. alterniflora* shown in Figure 4 is used in Figure 7. One can see that the drag coefficient of *S. alterniflora* is close to that of *J. roemerianus* with high h_v/h values, and larger than that of *J. roemerianus* with low h_v/h values. Overall, *S. alterniflora* has larger drag coefficient than *J. roemerianus*. This is due to different properties of these two vegetation species. One reason is that the cordgrass *S. alterniflora* has larger leaves than the needlegrass *J. roemerianus*. Another reason is that the stem diameter and population density of *J. roemerianus* vary more significantly along elevation.

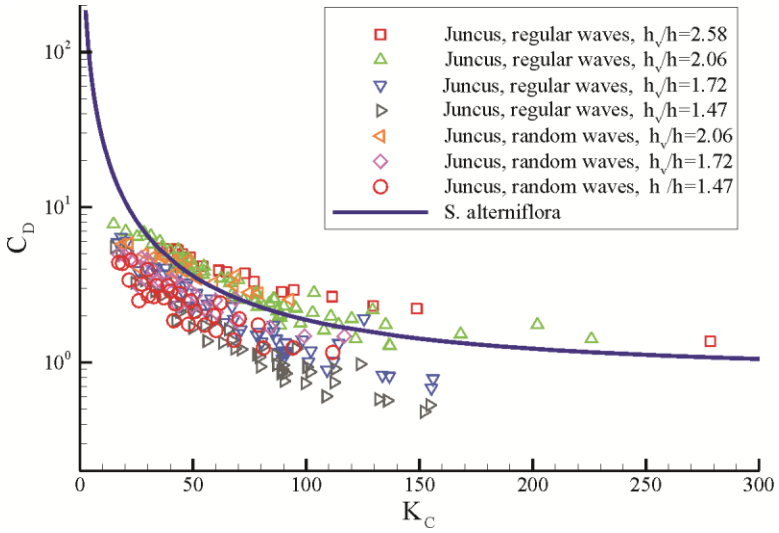

Figure 7. Comparison of drag coefficients of *S. alterniflora* and *J. roemerianus*.

6 CONCLUSIONS

Wave attenuation by live marsh vegetation was investigated in laboratory and field experiments. The laboratory experiments were conducted in a 20.6 m long, 0.69 m wide and 1.22 m deep wave flume under regular and random wave conditions. The vegetation species used in the laboratory experiments are *Spartina alterniflora* and *Juncus roemerianus*. *S. alterniflora* widely exists along the eastern, western and southern U.S. coastlines, while *J. roemerianus* is popular along coast of the Gulf of Mexico. The field measurements were conducted under high-energy conditions during the Tropical Storm Lee (September 3-4, 2011) at a salt marsh wetland in Terrebonne Bay on the Louisiana coast of the Gulf of Mexico, USA. The dominant vegetation on the field site was *S. alterniflora*.

The wave attenuation data were compared against the analytical models of Dalrymple et al. (1984) and Mendez and Loasada (2004). The bulk drag coefficient of vegetation was calibrated in each experiment run. The drag coefficient of *S.*

alterniflora is related to the Keulegan-Carpenter number, whereas the drag coefficient of *J. roemerianus* is related to the Keulegan-Carpenter number and vegetation submergence (ratio of vegetation height and water depth). The importance of vegetation submergence for *J. roemerianus* is due to that its stem diameter and density vary along the elevation. Regression equation is obtained for the drag coefficient of each tested vegetation species, and found to have good accuracy compared with the measured data.

It is recognized that Ozeren et al. (2015) obtained different relations for the drag coefficient of each vegetation species under regular and random waves in the laboratory experiments. In the present study, the data using regular and random waves collapse into single relation for each species by using the significant wave height and peak wave period as the representative parameters of random waves in the calculation of the Keulegan-Carpenter number. The newly derived relations of drag coefficient cover a wider range of wave conditions and combined regular and random wave data.

ACKNOWLEDGEMENT

The laboratory experiments and field measurements were supported by the Southeast Regional Research Initiative.

REFERENCES

Augustin, L.N., J.L. Irish, and P.L. Lynett (2009). Laboratory and numerical studies of wave damping by emergent and near-emergent wetland vegetation. *Coastal Engineering*, 56(3): 332-340.

Bendat, J.S., and A.G. Piersol (2000). *Random data: analysis and measurement procedures*, John Wiley and Sons, Inc. New York, NY.

Bradley, K., and C. Houser (2009). Relative velocity of seagrass blades: Implications for wave attenuation in low energy environments. *J. Geophys. Res*., 114: F01004, doi:10.1029/ 2007JF000951.

Chakrabarti, A., H.D. Smith, D. Cox, and D.A. Albert (2011). Investigation of turbulent structures in emergent vegetation under wave forcing. *Proceedings of the Coastal Sediments* (CS'11).

Chen, Q, and H. Zhao (2012). Theoretical models for wave energy dissipation caused by vegetation. *J. Engineering Mech*. doi:10.1061/(ASCE)EM.1943-7889.0000318.

Cooper, N.J. (2005). Wave dissipation across intertidal surfaces in the Wash Tidal inlet, Eastern England. *J. Coastal Res*., 21(1): 28-40.

Dalrymple, R.A., J.T. Kirby, and P.A. Hwang (1984). Wave Diffraction Due to Areas of Energy Dissipation. *J. Waterway, Port, Coastal and Ocean Engineering*, 110(1): 67–79.

Dubi, A., and A. Tørum (1996). Wave energy dissipation in kelp vegetation. *Proceedings of the 25th International Conference on Coastal Engineering* (ICCE 1996).

Kobayashi, N., A.W. Raichlen, and T. Asano (1993). Wave attenuation by vegetation. *J. Waterway, Port, Coastal and Ocean Engineering*, 119: 30–48.

Longuet-Higgins, M.S. (1952). On the statistical distribution of the heights of sea waves. *Journal of Marine Research*, 11(3): 245-266.

Lowe, R., J. Falter, J. Koseff, S. Monismith, and M. Atkinson (2007). Spectral wave flow attenuation within submerged canopies: Implications for wave energy dissipation. *J. Geophys. Res*., 112: C05018, doi:10.1029/2006JC003605.

Lowe, R.J., J.R. Koseff, and S.G. Monismith (2005). Oscillatory flow through submerged canopies: 1.Velocity structure. *J. Geophys. Res*., 110: C10016, doi:10.1029/2004JC002788.

Lövstedt, C.B., and M. Larson (2010). Wave damping in reed: Field measurements and mathematical modeling. *J. Hyd. Eng*., 136(4): 222-233.

Løvås, S.M., and A. Tørum (2001). Effect of kelp Laminaria hyperborea upon sand dune erosion and water particle velocities. *Coastal Eng*., 44: 37–63.

Mazda, Y., M. Magi, Y. Ikeda, T. Kurokawa, and T. Asano (2006). Wave reduction in a mangrove forest dominated by *Sonneratia sp*. *Wetlands Ecology and Management*, 14: 365–378.

Mendez, F.J., and I.J. Losada (2004). An empirical model to estimate the propagation of random breaking and nonbreaking waves over vegetation fields. *Coastal Eng*., 51: 103–118.

Mendez, F.J., I.J. Losada, and M.A. Losada (1999). Hydrodynamics induced by wind waves in a vegetation field. *J. Geophys. Res*., 104(C8): 18,383–18,396.

Möller, I. (2006). Quantifying salt marsh vegetation and its effect on wave height dissipation: results from a UK East coast saltmarsh. *Estuarine Coastal Shelf Sci*., 69: 337–351.

Möller, I., and T. Spencer (2002). Wave dissipation over macro-tidal salt marshes: effects of marsh edge typology and vegetation change. *J. Coast. Res*., SI36: 506–521.

Möller, I., T. Spencer, J.R. French, D. Leggett, and M. Dixon (1999). Wave transformation over salt marshes: a field and numerical modeling study from North Norfolk, England. *Estuarine Coastal Shelf Sci*., 49: 411–426.

Mullarney, J.C., and S.M. Henderson (2010). Wave-forced motion of submerged single-stem vegetation. *J. Geophys. Res*., 115: C12061, doi:10.1029/2010JC006448.

Pennings, S.C., M.B. Grant and M.D. Bertness (2005). Plant zonation in low-latitude salt marshes: disentangling the roles of flooding, salinity and competition. *J. Ecology*, 93: 159-167.

Ozeren, Y., D. Wren, and W. Wu (2014). "Experimental investigation of wave attenuation through model and live vegetation." Journal of Waterway, Port, Coastal, and Ocean Engineering (ASCE), 140(5), CID: 04014019, DOI: 10.1061/(ASCE)WW.1943-5460.0000251.

Quartel, S., A. Kroon, P.G.E.F. Augustinus, P. Van Santen, and N.H. Tri (2007). Wave attenuation in coastal mangroves in the Red River Delta, Vietnam. *J. Asian Earth Sci*., 29 (4): 576-584.

Stratigaki, V., E. Manca, P. Prinos, I.J. Losada, J.L. Lara, M. Sclavo, C.L. Amos, I. Cáceres, and A. Sánchez-Arcilla (2011). Large-scale experiments on wave propagation over Posidonia oceanica. *J. Hydraulic Res*., 49(sup1): 31-43.

University of Florida (2016). *Juncus roemerianus*. https://plants.ifas.ufl.edu/wp-content/uploads/images /junroe/junroe1m.jpg. Accessed on March 9, 2016.

Wikipedia (2016). *Spartina alterniflora*. https://en.wikipedia.org/wiki/Spartina_alterniflora#/media/File:Spartina_alterniflora.jpg. Accessed on March 9, 2016.

Wu, W., Y. Ozeren, D. Wren, Q. Chen, G. Zhang, M. Holland, Y. Ding, S.N. Kuiry, M. Zhang, R. Jadhav, J. Chatagnier, Y. Chen, and L. Gordji (2011). Investigation of surge and wave reduction by vegetation, Phase I Report for SERRI Project No. 80037, The University of Mississippi, MS, p. 315, with p. 465 Appendices.

Wu, W., Y. Ozeren, D. Wren, Q. Chen, G. Zhang, M. Holland, R. Marsooli, Q. Lin, R. Jadhav, K.R. Parker, H. Pant, J. Bouanchaud, and Y. Chen (2012). Investigation of surge and wave reduction by vegetation (Phase II) —Interaction of Hydrodynamics, Vegetation and Soil, Phase II Report for SERRI Project No. 80037, The University of Mississippi, MS, p. 395.